Hindawi
Advances in Materials Science and Engineering
Volume 2020, Article ID 6346590, 14 pages
https://doi.org/10.1155/2020/6346590

Research Article

Capacity of Cone-Shaped Hollow Flexible Reinforced Concrete Foundation (CHFRF) in Sand under Horizontal Loading

Shanshan Li,[1] **Yukun Zhang**,[2] **and Dayong Li**[3]

[1]*Centre of Offshore Geotechnical Engineering, Weifang University, Weifang 261061, China*
[2]*Key Laboratory of Civil Engineering Disaster Prevention and Mitigation, Shandong University of Science and Technology, Qingdao 266590, China*
[3]*College of Civil Engineering, Fuzhou University, Fuzhou 350108, China*

Correspondence should be addressed to Dayong Li; ldy@fzu.edu.cn

Received 16 April 2020; Revised 2 July 2020; Accepted 24 August 2020; Published 7 October 2020

Academic Editor: Georgios I. Giannopoulos

Copyright © 2020 Shanshan Li et al. This is an open access article distributed under the Creative Commons Attribution License, which permits unrestricted use, distribution, and reproduction in any medium, provided the original work is properly cited.

The cone-shaped hollow flexible reinforced concrete foundation (CHFRF) is an innovative type of mountain wind turbine foundation, which outperforms the regular mountain wind turbine foundation in reducing the steel and concrete and protecting the surrounding vegetation for the cavity absorbs soil obtained from excavating the foundation pit. Moreover, the rubber layer installed between the wall of CHFRF and the surrounding ground increases foundation flexibility and releases the larger overturning moment induced by wind. The rubber layer is made of alternately laminated rubber and steel. The objectives of this research are to study the lateral bearing behaviors of the CHFRF under monotonic and cyclic lateral loading in sand by model tests and FEM simulations. The results reveal that the CHFRF rotates during loading; and, in the ultimate state, the rotation center is located at a depth of approximately 0.6–0.65 times the foundation height and is 0.15–0.18 times the diameter of the foundation away from its centerline as well. The lateral bearing capacity of the CHFRF improves with the increase of embedded depth and vertical load applied to the foundation. Moreover, compared to the CHFRF without the rubber layer, the rubber layer can reduce the earth pressure along the wall of CHFRF by 22% and decrease the deformed range of the soil surrounding the foundation, revealing that it can reduce the loads transferred to the surrounding soil for extending the service life of the foundation. However, the thickness and stiffness of the rubber layer are important factors influencing the lateral bearing capacity and the energy dissipation of the foundation. Moreover, it should be noted that the energy dissipation mainly comes from the steel of the rubber layer rather than rubber.

1. Introduction

In China, it can be found that the on-land wind farms are currently moving from plain and desert areas to mountainous regions close to cities having high demand for electricity [1, 2]. It is because mountain wind farms do not occupy farmlands and have low construction cost of transmission lines, and the most important thing is that they will be conducive to the use of wind power to meet the rapid development and transformation of urban economy.

The gravity-based structure foundations [3], the rib-reinforced steel-concrete octagonal foundations [4], and the rock-bolted foundations are currently used as the foundations of the mountain wind turbines [5], and the circular gravity-based foundation (CGF) is the most common type used in mountain wind turbine projects. However, it should be noted that the aforementioned foundations have some disadvantages; for example, the usage quantities of steel bar, poles, and concrete are very large, resulting in a high cost; and concrete cracks occur due to autogenous shrinkage and thermal effects during the concrete casting, increasing the risks of water ingress in the foundation and corrosion of steel bars in reinforced concrete and thus significantly decreasing the bearing capacity of the foundations [6]. In addition, it was reported that some damage for the wind turbine tower was caused by forming a plastic hinge subjected to harsh wind load [4, 5]. Also, we found that the soil will be piled up near the foundation pit excavation, spoiling growth of vegetation as well.

Therefore, in order to tackle these problems for the above-mentioned regular foundations, a novel type of mountain wind turbine foundation, the cone-shaped hollow flexible reinforced concrete foundation (CHFRF), was proposed by Li et al. [7]. The sketch of the CHFRF is shown in Figure 1. It can be seen that its cavity is packed with vast quantities of soil that has been excavated from the ground pit; thus, the CHFRF will absorb much spoil for protecting the surrounding vegetation and can considerably reduce the usage quantity of concrete and steel bars compared with the regular mountain wind turbine foundations. Besides, the rubber layer is placed beneath the CHFRF to increase the foundation flexibility. However, in order to eliminate the weathered and aging effects and to increase the stiffness and service lifetime of rubber, steel layers are added in the rubber layer. Thus, the rubber layer is made of alternately laminated rubber and steel. Furthermore, it is found that the turbine tower is directly connected to the CHFRF by using many high-performance steel anchors. Our previous work indicates that the concrete volume of CHFRF is reduced by 79%, and the backfilled quantities of the soil increase 2 times compared to the corresponding CGF under the same diameter and height foundation. It is also found that, under horizontal monotonic loading, the bearing capacities of the CHFRF with the eccentricities of 0.75, 1.0, and 1.25 increased by approximately 29.3%, 43.75%, and 43.75%, respectively, compared with the circular gravity-based foundation. Moreover, the experimental results show that the accumulated rotation of CHFRF with rubber thickness layer changing from 2 to 4 mm is effectively decreased under cyclic loading. These results can be referred to our paper in Soils and Foundations [7].

The mountain wind turbine foundations are generally required to withstand larger lateral loads and moment resulting from wind, which play a predominant role in the design of the foundation. Although the CHFRF is a new type of mountain wind turbine foundation, we can borrow some ideas from the conventional foundations to reveal its bearing responses under lateral loading; for example, Gajan and Kutter [8] and Adhikari and Bhattacharya [9] investigated the influence of foundation-soil contact models on the lateral bearing capacity of the CGF by model tests, and it was found that the deformation behavior of the soil located at the bottom of the CGF is significantly affected by the form of wind load, varying the lateral bearing capacity of the foundation [10]. Furthermore, Govoni et al. [11] proposed the expression to obtain the ultimate horizontal bearing capacity of the CGF embedded in dense sand and then studied the effects of sand density and size on the horizontal bearing capacity of the foundation [12]. Besides, the influence of vertical load, embedded depth, and soil mechanical parameters on the ultimate horizontal bearing capacity of the foundation and soil deformation was studied by Mohamed and Cerato [13, 14], respectively. In addition, the relationships between earth pressure, foundation stiffness and soil mechanical parameters, and the ultimate horizontal bearing capacity, respectively, were studied by Décourt and Vahdatirad [15, 16].

In this study, a series of model tests and FEM simulations were conducted to further obtain the bearing behaviors of the CHFRF with different diameter and height under monotonic and cyclic lateral loading with various load eccentricities, respectively. The effects of embedment depths and vertical load on lateral bearing capacity of the CHFRF were obtained as well. Moreover, during lateral loading, the distributions of rotation center of the CHFRF and earth pressures along the wall of CHFRF were revealed. Furthermore, the effects of thickness of the rubber layer on lateral bearing capacity and energy dissipation capacity of the CHFRF in sand were analyzed in detail.

2. Preparation of Model Tests

2.1. Test Equipment

2.1.1. Foundation Models. The foundation models are made of steel (Figure 2), without considering forces within the foundation during loading. The dimensions of the CHFRF models are shown in Table 1, while for the CGF height (H) is 60 mm and the diameter (D) is 300 mm (Figure 2(a)). The dimension of the prototype CGF is from Qingdao, China, and the dimension ratio of the model to prototype is 1 : 60.

2.1.2. Testing Instruments. As shown in Figure 3, the tank is 1 m long, 1 m wide, and 0.8 m high, which is large enough to eliminate boundary effects [17]. Also, it can be found that the lateral loads were measured by a load cell and the corresponding horizontal deflection was measured by a horizontal LVDT. In addition, two vertical LVDTs (the measuring accuracy is 0.01 mm) with an interval distance of 17 cm were vertically placed on the top plate of the foundation to measure the vertical displacement of the foundation during loading. Moreover, there is an inclinometer located at the loading rod to get the rotation angle of CHFRF, and the measuring accuracy of the inclinometer is 0.01°. Besides, eight earth pressure cells (the maximum is 50 kPa and the measuring accuracy is 0.01 kPa) were attached to the wall of CHFRF for revealing the relationship between earth pressure and horizontal deflection of the CHFRF during loading.

2.2. Sand Used. The natural medium coarse sand used in this study was collected from a mountainous area of Qingdao in East China, and its particle size distribution curve is shown in Figure 4. The results show that the unevenness coefficient (C_u) and the curvature coefficient (C_c) are equal to 6.17 and 1.63, respectively. In addition, the maximum and minimum void ratios of sand are 0.663 and 1.102, respectively, and the specific gravity of sand is 2.685. These tests were conducted according to ASTM C127 [18]. Furthermore, based on the standard penetration test (SPT) [19], the standard penetration test number of the in situ sand is less than 50. Therefore, the engineering properties of the sand used are close to those of fully and strongly weathered granite, which is one of the commonly used soil foundations for mountain wind turbines.

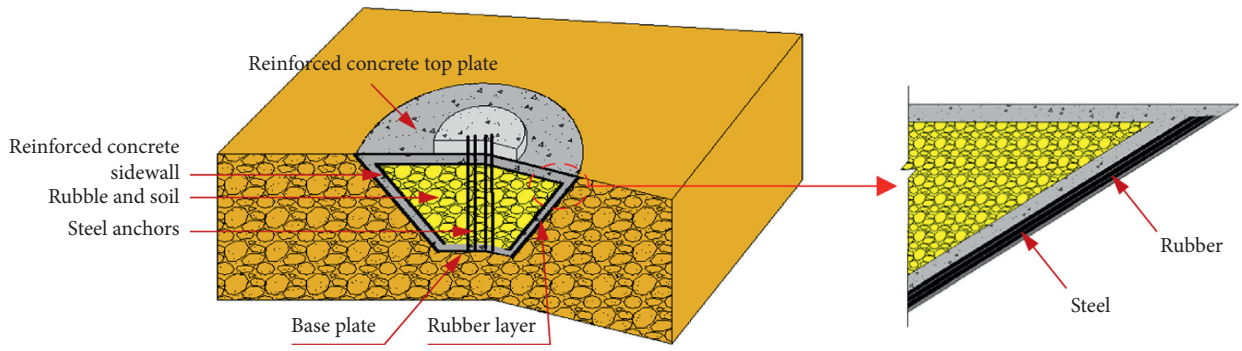

Figure 1: Sketch of the CHFRF.

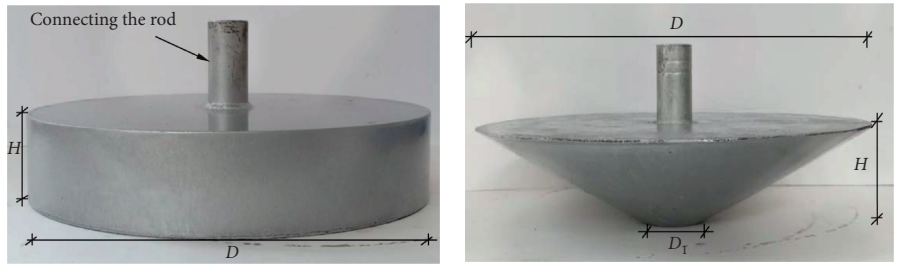

(a) (b)

Figure 2: Foundation models. (a) Circular gravity-based foundation model. (b) CHFRF model.

Table 1: Dimensions of the foundation models.

Dimensions	Circular gravity-based foundation	Nos. of CHFRF			
		II-A	II-B	II-C	II-D
D (mm)	300	300	300	360	400
D_1 (mm)	300	0	85	85	0
H (mm)	60	60	60	72	80
Weight (N)	85	52	56	72	81

2.3. Testing Procedure. Gravel with particle size range of 10~25 mm is initially placed uniformly to a thickness of 15 cm to form the filter layer located at bottom of the sand tank. Above the filter layer, there is a sheet of geotextile with the thickness of 2 mm to prevent sand from washing away. Furthermore, in order to conveniently control the thickness of the fill and its corresponding relative density, we marked every 5 cm on the side wall of the tank until the height of 60 cm is reached. In addition, in order to make the tests reproducible, it is necessary to keep the testing condition as unchanged as possible and the error range of the ultimate limit state load within 5%.

Therefore, one half of the sand in the testing tank was then loosened to a depth of two times the diameter of the foundation. Subsequently, a 2.5 kg mass used as the compacting hammer is dropped from a height of 30.5 cm above the sand, and the sand in the range of 2 times the diameter of the top lid of foundation was compacted. The sand in each compacted position should be continuously hammered 30 times. Finally, the foundation models are laid in sand for about 3 h before initiating the tests for ensuring that the settlement of the foundation is completed. The relative density and the density of sand were tested as 0.52 and 1600 kg/m^3, respectively, and the unit weight equals 16 kN/m^3. Moreover, the shear strength of sand was obtained using the CDS ShearTrac-II and equals 40 kPa.

In addition, incremental horizontal loads were applied at various loading eccentricities, e, presenting the distance between the loading position and the lid surface of the foundation. In this study, the loading eccentricities equal 22.5, 30, and 37.5 cm, respectively, and the lateral load was applied by using the self-designed servo loading device, which can divide the lateral load into many incremental load steps, while until the horizontal deflection of the foundation measured by the horizontal LVDT to be less than 0.01 mm/min, the next load is applied. Besides, it should be noted that the foundation tilts up to 3°, indicating the termination of the tests.

3. Tests Results and Discussion

It is found that the normalized 1 g laboratory test results for the wind turbine foundation under lateral loading can be scaled to the field in most cases to widely explore the range of conditions and factors that influence the bearing capacity and can also apply the results from model tests to practical engineering [20–22]. Therefore, the lateral load and the corresponding horizontal deflection are normalized as $F^2/(2\pi R^5\gamma\tau)$ and u/D, respectively, where F is the applied lateral load, u is the deflection of the foundation, and R and D are the radius and diameter of the foundation, respectively. Besides, γ and τ are unit weight and the shear strength of the

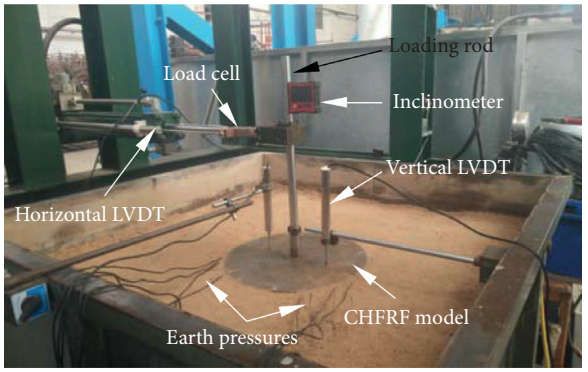

Figure 3: Model test setup.

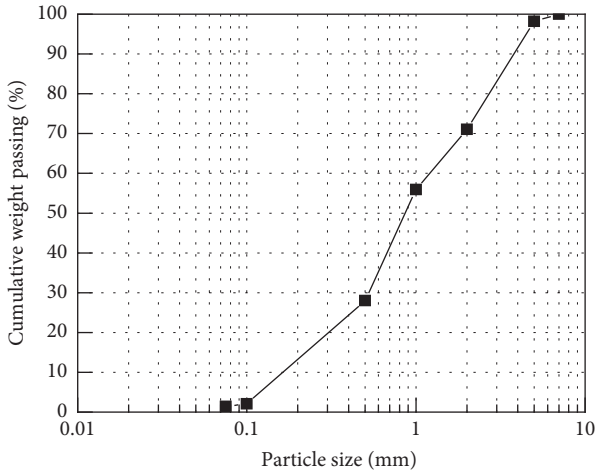

Figure 4: Particle size distribution curve.

soil, respectively. In the next section of this paper, all model tests results are presented in normalized form. In addition, Figure 5 gives the lateral load-horizontal deflection curves of the CHFRF no. II-A with e of 22.5 cm. It can be seen that test results are credible for the error range of the lateral bearing capacity within 5%.

3.1. Effects of Dimensions of CHFRF on the Lateral Bearing Capacity. To investigate the effects of dimensions of the CHFRF's lid, floor base and height, the load eccentricity (e), the embedded depths, and vertical loads on the horizontal bearing capacity, model tests were conducted on both the CHFRF and the CGF under e of 22.5 and 37.5 cm, respectively, and the tests' results are shown in Figures 6 and 7 (the value of embedded depth ratio, d/D, is equal to zero).

As shown in Figure 6, it can be found that the variation of the lateral load-horizontal deflection curves is the same, whereas the size and the weight of the foundation significantly influenced the bearing capacity of the foundation. In the case of the same diameter and height, the lateral bearing capacities of CHFRF nos. II-A and II-B are both slightly less than that of the CGF. The reason is that the weights of CHFRF nos. II-A and II-B are about 70% of the weight of the CGF under the same foundation size, causing the lateral

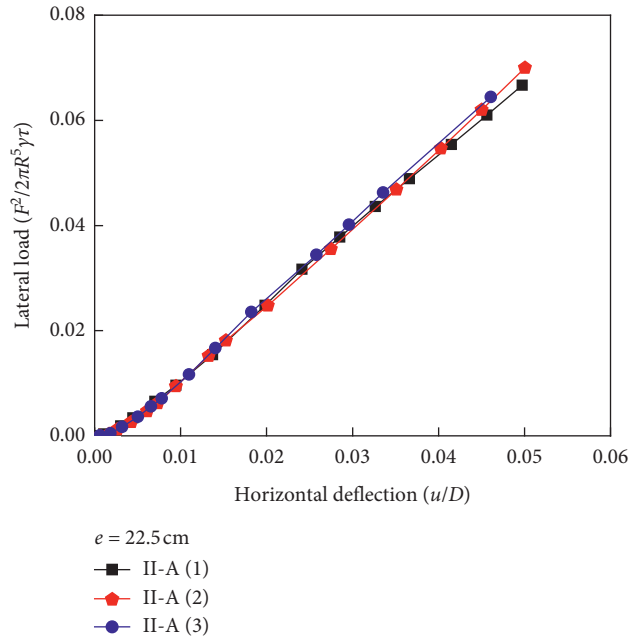

Figure 5: Lateral load versus horizontal deflection.

bearing capacities of CHFRF nos. II-A and II-B to be slightly less than that of CGF. Besides, for CHFRF no. II-C, its weight decreases by 15% compared with the corresponding CGF, whereas its lateral bearing capacity increases by 10% compared to that of CGF. In addition, for CHFRF no. II-D, its self-weight is approximately equal to the weight of CGF, while its lateral bearing capacity is extended by 30% compared to that of CGF. It is because when in the case of the foundation with the same weight, the size of CHFRF no. II-D is increased, resulting in the considerable increase of interface between the foundation and the soil surrounding the foundation, and then the bearing capacity significantly improved. Therefore, it can be concluded that the CHFRF mainly relies on increasing the interface between the foundation rubble and soil to improve the bearing capacity.

From Figure 6, it is also found that the CHFRF significantly decreases the horizontal deflection compared to that of the CGF within the same value of lateral load; for example, under the normalized lateral load of 0.04, the lateral bearing capacities of CHFRF nos. II-C and II-D approximately reduce by 35% and 57%, respectively. Therefore, the CHFRF increases the lateral bearing capacity and reduces the horizontal deflection of the foundation as well, compared to the corresponding CGF under the same value of lateral load.

3.2. Effects of Embedded Depth of CHFRF on the Lateral Bearing Capacity. The foundation embedded depth has an important influence on the lateral bearing capacity of the foundation. In order to investigate the effect of embedded depth of the CHFRF on the bearing capacity, model tests on the CHFRF no. II-A with embedded depth ratio (d/D) of zero, 0.05, and 0.1 were conducted, respectively. From Figure 7(a), it can be noted that the lateral bearing capacity of CHFRF approximately increases by 50% as d/D changes

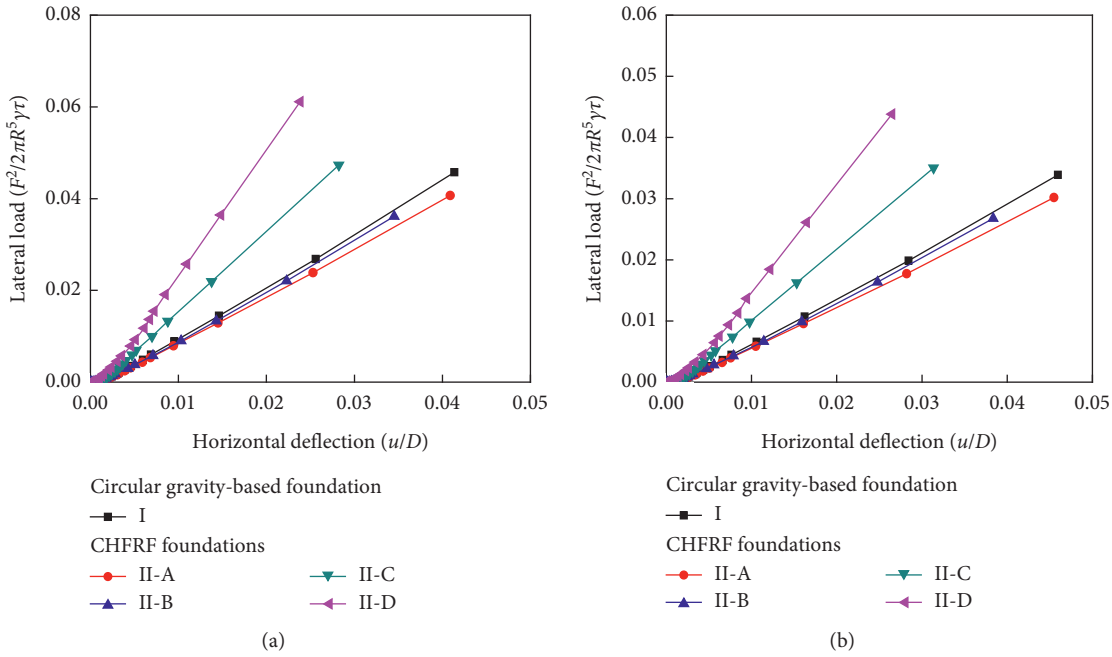

Figure 6: Relationship between lateral load and horizontal deflection ($d/D = 0$). (a) $e = 22.5$ cm. (b) $e = 37.5$ cm.

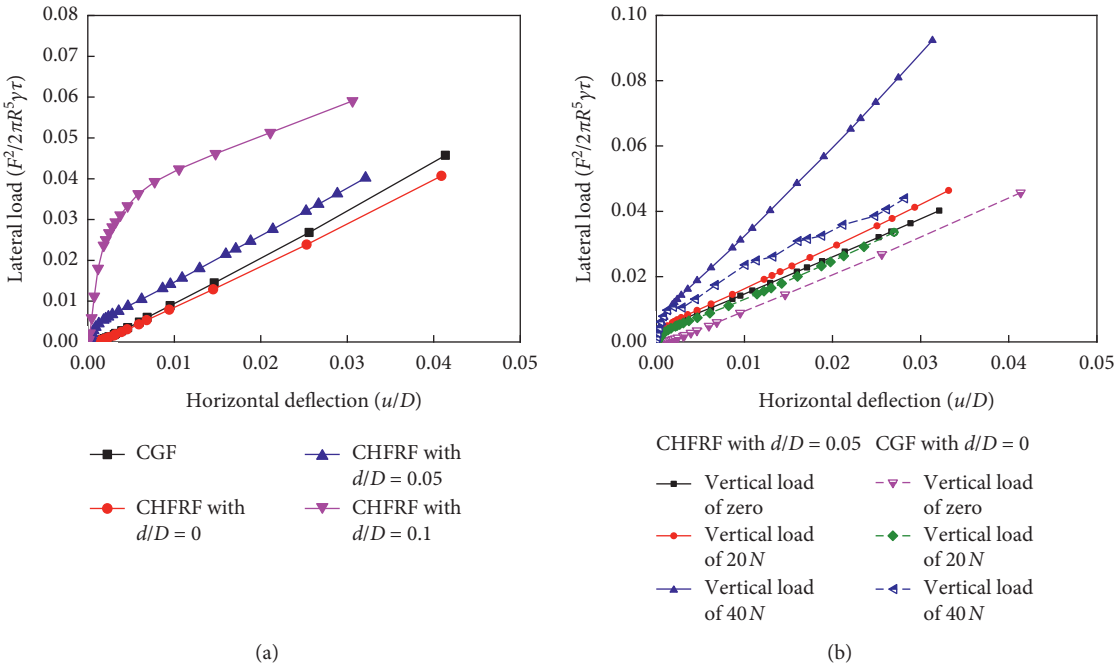

Figure 7: Effects of embedded depth on the lateral bearing capacity. (a) Vertical load of zero. (b) Vertical load range from 20 N to 40 N.

from zero to 0.1. Moreover, the results show that the lateral bearing capacity of CHFRF is less than that of CGF under the same values of foundation diameter and height, while its values are greater than the corresponding CGF in the case of embedded depth ratio being equal to 0.05 and 0.1, revealing that the embedded depth ratio significantly influences the lateral bearing capacity of the CHFRF. Besides, as shown in Figure 7(b), it can be seen that the lateral bearing capacity of CHFRF is greater than the corresponding CGF as the vertical load increases from 20 N to 40 N under the same value of embedded depth ratio. Therefore, it can be concluded that the lateral bearing capacity of CHFRF significantly increases with the increase of the embedded depth and vertical load, and its values are larger than the corresponding CGT under

the same diameter and height (except for the case when the values of embedded depth and vertical are both equal to zero).

3.3. Effects of Load Eccentricity on Lateral Bearing Capacity. Figures 8(a) and 8(b) represent the effects of loading eccentricity (e) on the horizontal bearing capacity of CHFRF nos. II-C and II-D, respectively. The results reveal that, with the increase of load eccentricity, there is a considerable decrease in bearing capacity under the same value of lateral deflection; for example, when the values of loading eccentricity change from zero to 37.5 cm, the lateral bearing capacity of CHFRF no. II-D appropriately decreases by 12%~50%. The reason for the reduction in the lateral bearing capacity is that the overturning moment acting on the CHFRF significantly increases with the load eccentricity increasing.

3.4. Distribution of the Rotation Centers for CHFRF. According to the experimental observation of the tests results, it is found that the CHFRF rotates about a point (rotation center) during loading (Figure 9). Based on the vertical displacement of the foundation lid, the deviation between the rotation center and the centerline of the foundation (s) can be calculated by equation (1). Besides, based on the horizontal deflection of the loading point and the rotation angle of CHFRF, the distance between the surface lid and the rotation center in the vertical direction (h_2) can be calculated by equation (2). Furthermore, the changing characters of vertical displacement for the foundation with the increase of the horizontal displacement of the foundation are shown in Figure 10.

$$s = R \cdot \frac{v_1 - v_2}{v_1 + v_2}, \tag{1}$$

$$h_2 = \frac{a - s}{\tan\theta} - h_1, \tag{2}$$

where R is the radius of the foundation, v_1 and v_1 refer to the vertical displacement of the lid of the foundation at opposite the loading direction and the loading direction, respectively, θ is the rotation angle of the foundation during loading, and h_1 refers to the distance between the loading position and the lid of the foundation.

Based on the rotation center position, the failure mechanism of the CHFRF and the active and passive earth pressure zones along the wall of CHFRF can be well understood during lateral loading process, and then the appropriate assumption and the analysis model will calculate the ultimate lateral bearing capacity of the CHFRF. Figures 11 and 12 give the distribution of rotation center positions. From Figure 11, the research results reveal that the rotation center moves to the loading direction with the increase of horizontal deflection of the CHFRF and then gradually tends to be stable with the increase of the lateral loading. Moreover, in the loading direction, the rotation center lies in approximately 0.15–0.18D under the load eccentricity e = 22.5, 30, and 37.5 cm, while the rotation center position of the CGF significantly varies during loading. Besides, the rotation center position also moves upward during loading (Figure 11). Furthermore, in the limit sate, the rotation center of the CHFRF is located at the embedded depth of 0.6–0.65 times the height of the foundation (Figure 11). On the other hand, based on the results of Figures 11 and 12, it can be observed that the loading eccentricity is a key influencing factor in the rotation center distribution of the CHFRF compared with that for the CGF.

3.5. Distribution of Earth Pressure along the Wall of CHFRF. In order to measure the incremental earth pressure along embedded depth during lateral loading, eight miniature earth pressure cells (the dimensions of earth pressure cells are 5 mm in diameter and 2 mm in thickness) were embedded along the wall of CHFRF. The experimental results presented in Figure 13 indicate the relationships between earth pressures and the embedded depths in the lateral loading direction and opposite the loading direction, respectively.

As shown in Figures 13(a), it can be seen that the Earth pressure located at the depths of 10, 25, 45, and 65 mm below the lid of CHFRF is positive in the loading direction, revealing that these earth pressure cells are in the passive earth pressure zone. However, these values of earth pressures firstly increase and then decrease with the embedded depth increasing, and the maximum value of the incremental earth pressure is obtained on the embedded depth of 0.3H (approximately 25 mm). In addition, opposite the loading direction, the distribution of the earth pressures slightly increases with the embedded depth increasing, while the values of these earth pressure cells are smaller than 1.5 kPa (Figure 13(b)). It should be noted that earth pressures along the embedded depths range of 0.64H below the foundation lid are close to or equal to zero. Therefore, it is concluded that the superstructure of CHFRF is the main part for bearing loads, which can be used to guide the position of rubber layer along the wall of CHFRF.

4. Effects of Rubber Layer on Bearing Behaviors of CHFRF

In model testing, a rubber layer with thickness of 2 mm is attached to the CHFRF wall to be used as the flexible layer (Figure 14), and its shore hardness (H_A) is equal to 35, 43, and 50, respectively. The shore hardness (H_A) can reveal the hardness of a metal or of a plastic or rubber material, and lower hardness is generally less stiff and will feel softer or spongier to the hand [23]. In order to improve the engineering design of rubber, the relationship between the shore hardness degrees with elastic moduli is built based on elastic theory (equation (3)) [24]. Thus, based on the expression of equation (3), the elastic moduli (E_{rubber}) of rubber used in this study are 1.400, 1.898, and 2.465 MPa, respectively.

$$E_{\text{rubber}} = \frac{15.75 + 2.15H_A}{100 - H_A}. \tag{3}$$

Subsequently, the loading-deflection tests were conducted to study the effects of rubber layer on the lateral

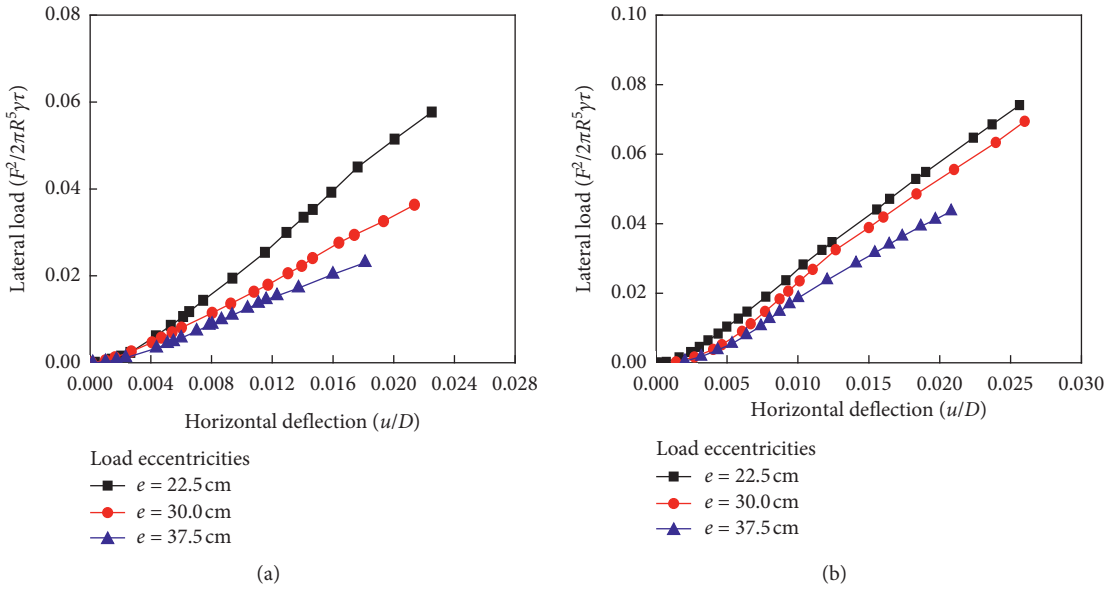

Figure 8: Effects of load eccentricities on lateral bearing capacity of CHFRF. (a) No. II-C. (b) No. II-D.

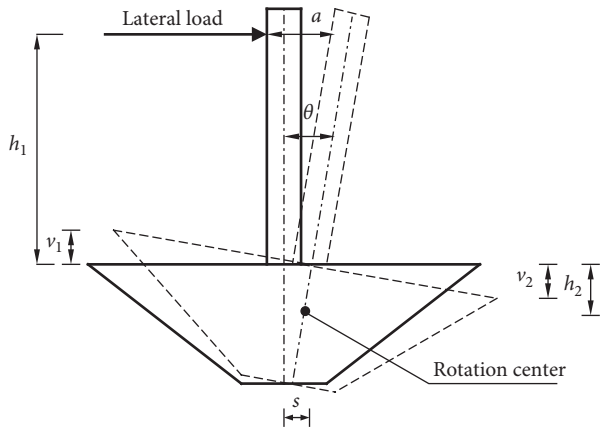

Figure 9: Sketch of rotation center position.

bearing behaviors of CHFRF. It can be seen that the horizontal bearing capacity of the CHFRF with a rubber layer decreases approximately by 8%, compared with the corresponding measured values of the CHFRF without a rubber layer when e equals 22.5 cm (Figure 15(a)). Besides, as the elastic modulus of rubber, E_{rubber}, increases from 1.4 to 2.465 MPa, there is a significant reduction in the lateral bearing capacity of CHFRF.

Figure 15(b) gives the effects of the rubber layer with different elastic moduli on the earth pressures along the wall of CHFRF (the maximum value of earth pressure obtained on the embedded depth of 0.31H). The results indicate that the rubber layer effectively decreases the Earth pressure along the wall of CHFRF during loading. It is because the lateral load is initially transferred from the CHFRF to the flexible rubber layer, resulting in the volume deformation of the rubber and then causing the rotation of CHFRF. Subsequently, the loads can be transferred to the surrounding soil, causing the corresponding deformation of the ground. However, because the rubber layer absorbs part of the lateral load by its volume deformation, the earth pressure decreases by 22% compared to that without a rubber layer. Furthermore, the results also reveal that the smaller the rubber elastic modulus is, the more the value of the earth pressure acting on the CHFRF wall decreases.

5. Numerical Modeling

To further explore the effects of the rubber layer on both the bearing capacity and energy dissipation of the CHFRF, five cases of different thickness were investigated by conducting the ABAQUS software. Moreover, the finite element method can help visualize the deformation of the soil surrounding the foundation. Thus, a three-dimensional numerical model is used to study the effect of the rubber layer on the bearing capacity and energy dissipation under cyclic lateral loading. Besides, it is reported that the vertical load applied to the foundation of a 2 MW wind turbine is approximately 500 kN. Thus, the numerical simulations were conducted for revealing the lateral load displacement of the foundation under vertical load of 500 kN.

5.1. Finite Element Model. Figure 16 represents a typical mesh and boundary extensions of the sand domain for the CHFRF with the rubber layer. The dimension of sand domain should be chosen to be sufficiently large enough to avoid boundary effects. Li et al. concluded that soil domain dimensions of 10 D in diameter and 6 D in height could reduce the boundary effects, where D is the diameter of the foundation [7]. The sizes of the CHFRF and the thickness of the rubber layers are shown in Table 2.

5.2. Constitutive Model and Sand Parameters. Analysis of 3D bearing capacity of the CHFRF in sand is performed using the Mohr–Coulomb failure criterion. The mechanical

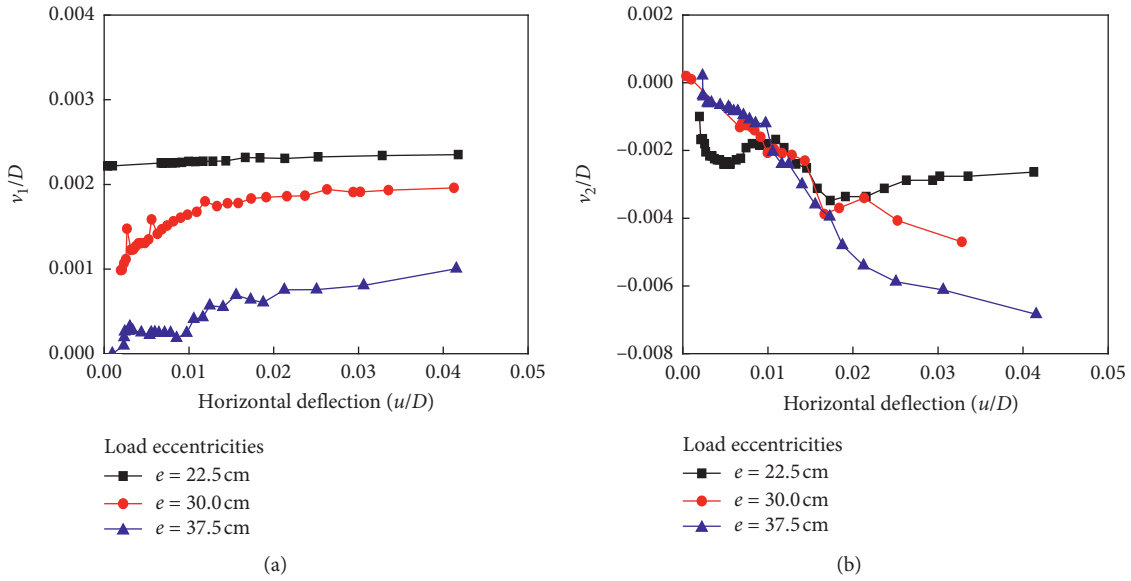

Figure 10: Vertical displacement of the CHFRF no. II-D under lateral loading. (a) For the distribution of v_1. (b) For the distribution of v_2.

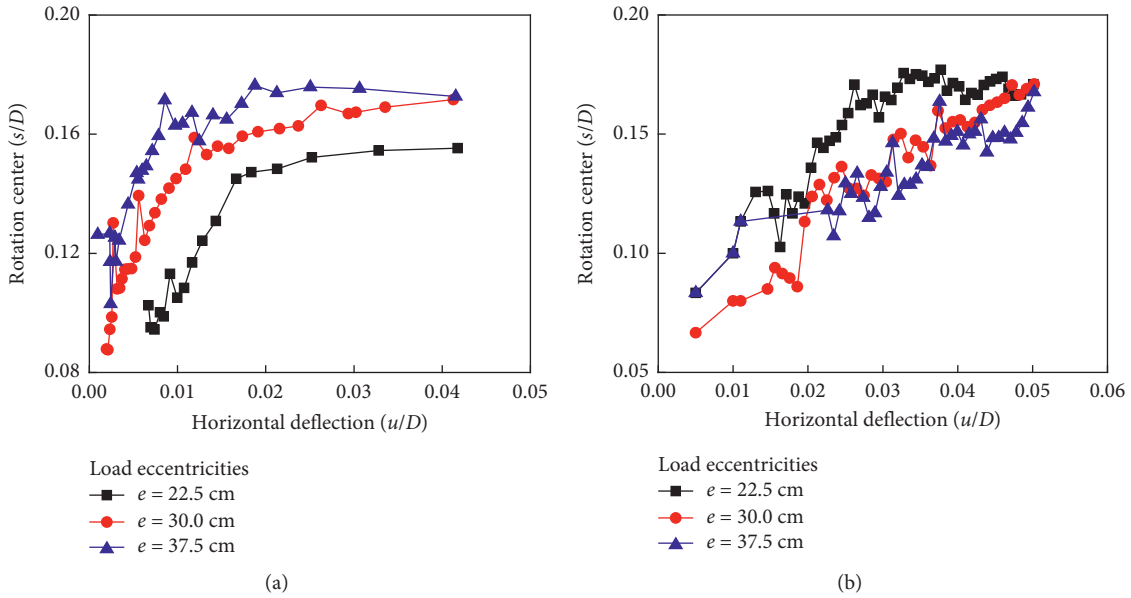

Figure 11: Rotation center distribution in the loading direction. (a) For the CHFRF no. II-D. (b) For the circular gravity-based foundation.

parameters of sand are as follows: the angle of internal friction $\varphi = 34^\circ$, the cohesion $c = 1$ kPa, the dilatation angle $\psi = 16^\circ$, and deformation modulus $E_0 = 10\,\text{N/mm}^2$. These mechanical parameters of sand are obtained by using the direct/residual shear test apparatus (ShearTrac-II), and the sand used is collected from the sand tank of the model test. The mechanical parameters of the foundation such as elastic moduli, Poisson's ratio, and the unit weight are equal to 30 GPa, 0.3, and $25\,\text{kN/m}^3$, respectively [25]. Besides, it should be noted that penalty finite elements are set up in the contact part between the foundation and sand, and the corresponding interface friction angle δ equals 28.8° determined by using the GDS interface shear apparatus [26]. Besides, for numerical simulations of rubber behaviors, the Mooney-Rivlin failure criterion is used in this study. Poisson's ratio and the unit weight of rubber are equal to 0.4999 and $14\,\text{kN/m}^3$, respectively [27]. The mechanical parameters of ABAQUS's super-elastic material model are as follows: $C_{10} = 0.17615$ MPa, $C_{01} = 0.438200$ MPa, and $D_1 = 0.0001$ [27]. Moreover, the mechanical parameters of steel such as elastic moduli, Poisson's ratio, and the unit weight are equal to 210 GPa, 0.3, and $70\,\text{kN/m}^3$, respectively [28].

5.3. Results and Discussion of FEM Simulations. Firstly, in order to verify the accuracy of numerical simulation results, a comparison between the numerical simulation and the

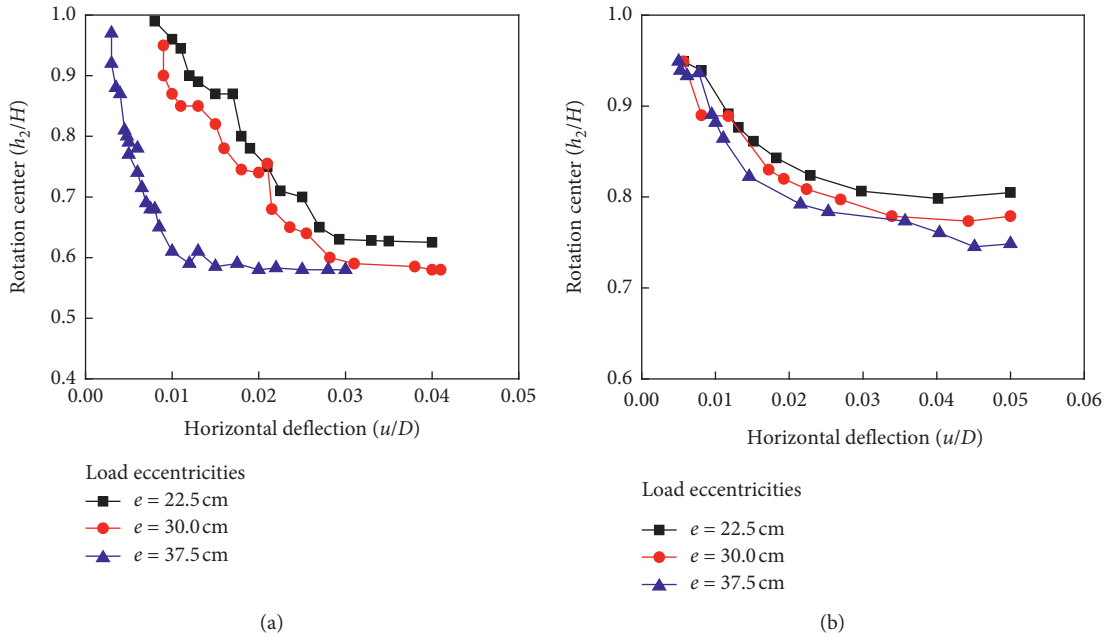

Figure 12: Rotation center distribution in the embedded depth. (a) For the CHFRF no. II-D. (b) For the circular gravity-based foundation.

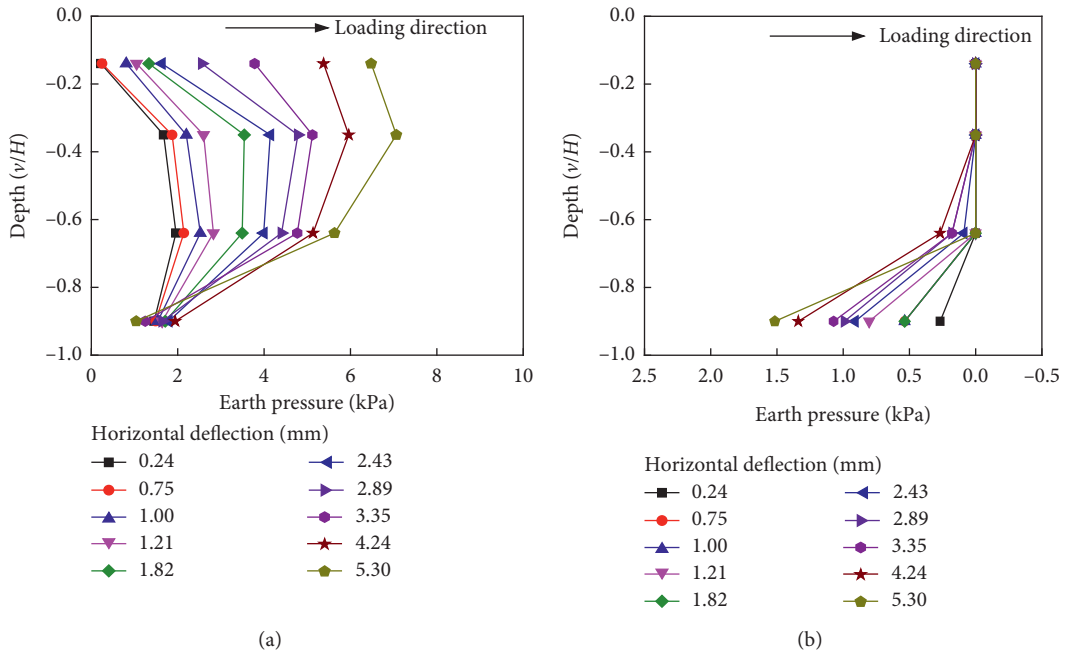

Figure 13: Distribution of earth pressure along CHFRF no. II-D. (a) In the loading direction. (b) Opposite the loading direction.

experimental results is conducted for the CHFRF nos. II-C and II-D with the loading eccentricity of 37.5 cm (Figure 17). From Figure 17, it can be concluded that the results of numerical solution are in good agreement with experimental results.

Subsequently, we carry out a numerical simulation analysis of the CHFRF with the sizes shown in Table 2 under monotonic and cyclic lateral loading. The results are shown in Figures 18 and 19. It can be found that, under the vertical load of 500 kN, the lateral bearing capacity of CHFRF decreases with increasing the thickness of the rubber layer without steel inside, while the value of the lateral bearing capacity tends to be stable when the thickness of rubber is greater than 20 mm (Figure 18). Also, it is found that the lateral bearing capacity increases with the steel thickness increasing; for example, the lateral bearing capacity of the CHFRF with the rubber layers no. 4 and no. 5 is approximately 1.68 times and 1.39 times greater than that of the

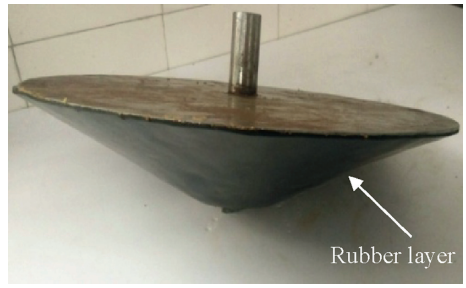

Figure 14: CHFRF with the rubber layer.

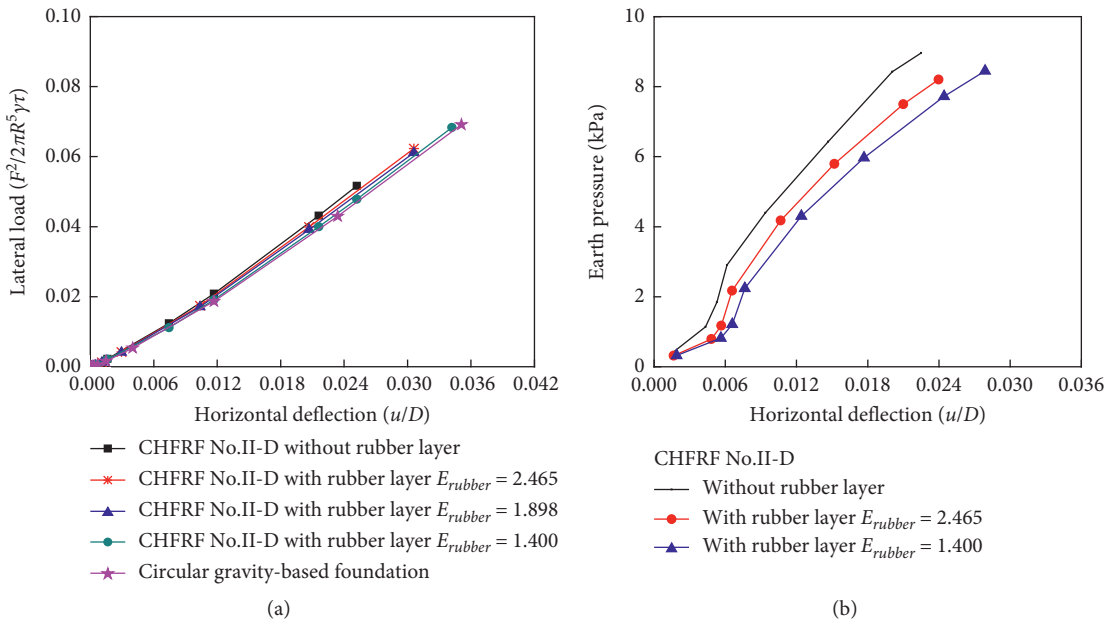

Figure 15: Effects of a rubber layer on the lateral bearing behaviors. (a) Lateral load versus deflection. (b) Earth pressure versus deflection.

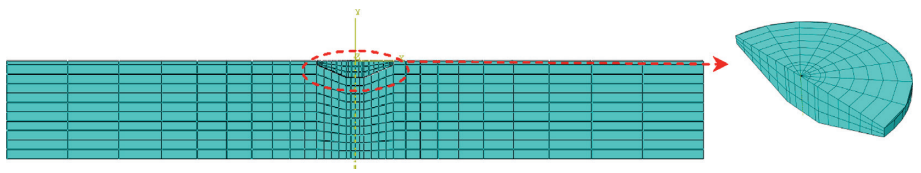

Figure 16: Finite element model.

Table 2: Dimensions of the foundation and the thickness of rubber layers.

Foundation dimensions		Nos. of rubber layers with different thickness						
D (m)	22	1	2	3	4		5	
D_1 (m)	4.5	Rubber	Rubber	Rubber	Rubber	Steel	Rubber	Steel
H (m)	4.4	10 mm	20 mm	30 mm	20 mm (10 mm/each layer)	10 mm	30 mm (10 mm/each layer)	20 mm (10 mm/each layer)

CHFRF without the rubber layer, respectively. Thus, it can be concluded that the thickness of rubber and steel is an important factor influencing the lateral bearing capacity of the foundation in sand.

On the other hand, during 10 numbers of lateral cyclic loading, the load-displacement curves of the CHFRF with different thickness of rubber layer are shown in Figure 19. The energy dissipation capacity of CHFRF can be evaluated

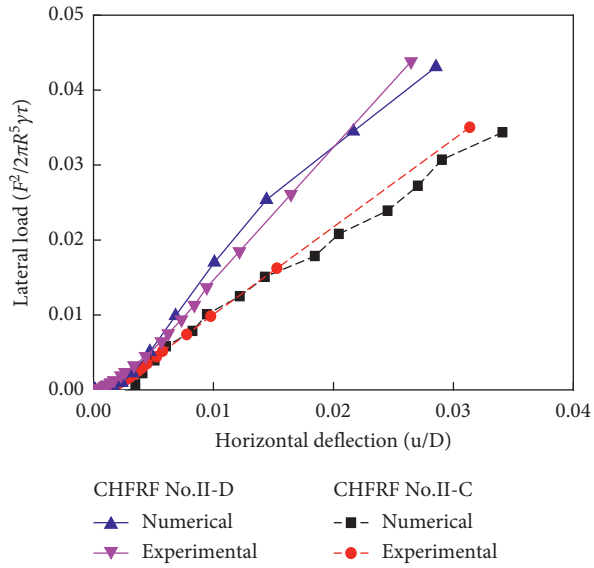

Figure 17: Comparison between test and numerical simulation results.

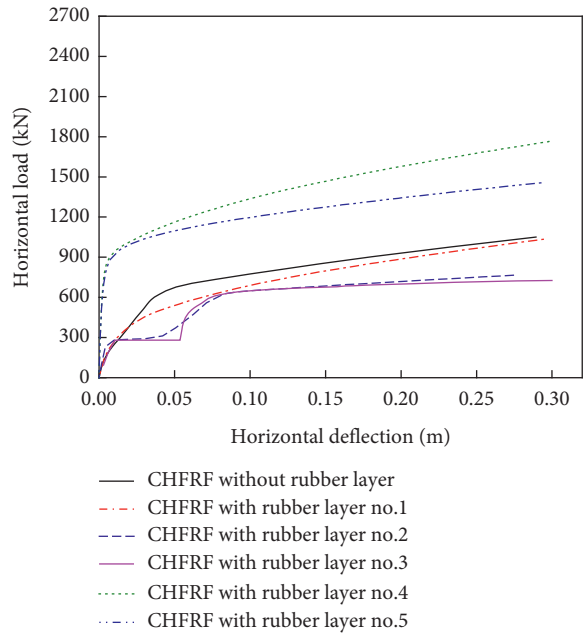

Figure 18: Effects of rubber layer on the lateral bearing capacity.

by calculating the area of load-displacement envelope curves. Generally, the larger the value of the area of load-displacement envelope curves, the higher the energy dissipation capacity of CHFRF under cyclic loading. From Figure 19, it can be seen that the rubber layer has a significant impact on the energy consumption of the CHFRF, compared to the corresponding the CHFRF without the rubber layer. Moreover, there is a greater energy dissipation capacity for the CHFRF in the case when the rubber layer has steel inside (Figure 19(d)), compared to the case where the rubber layer does not have steel (Figures 19(b) and 19(c)). The results also show that the energy dissipation mainly comes from the steel of the rubber layer rather than rubber. However, these results apply to the CHFRF with the rubber layer in sand under lateral loading. A detailed discussion of the optimal thickness of the rubber layer should be further conducted in various loading cases and various parameters of the soil, especially in the ground mixed by the rock mass.

In addition, the deformed ranges of the soil around CHFRF in cyclic loading are shown in Figure 20. The results show that the deformed range of the soil around the CHFRF with the rubber layer is significantly smaller than that of the CHFRF without the rubber layer, presenting that the rubber layer can reduce the deformation of the soil surrounding the foundation. This is because the rubber layer is flexible, and its energy dissipation capacity is strong, which plays a role in

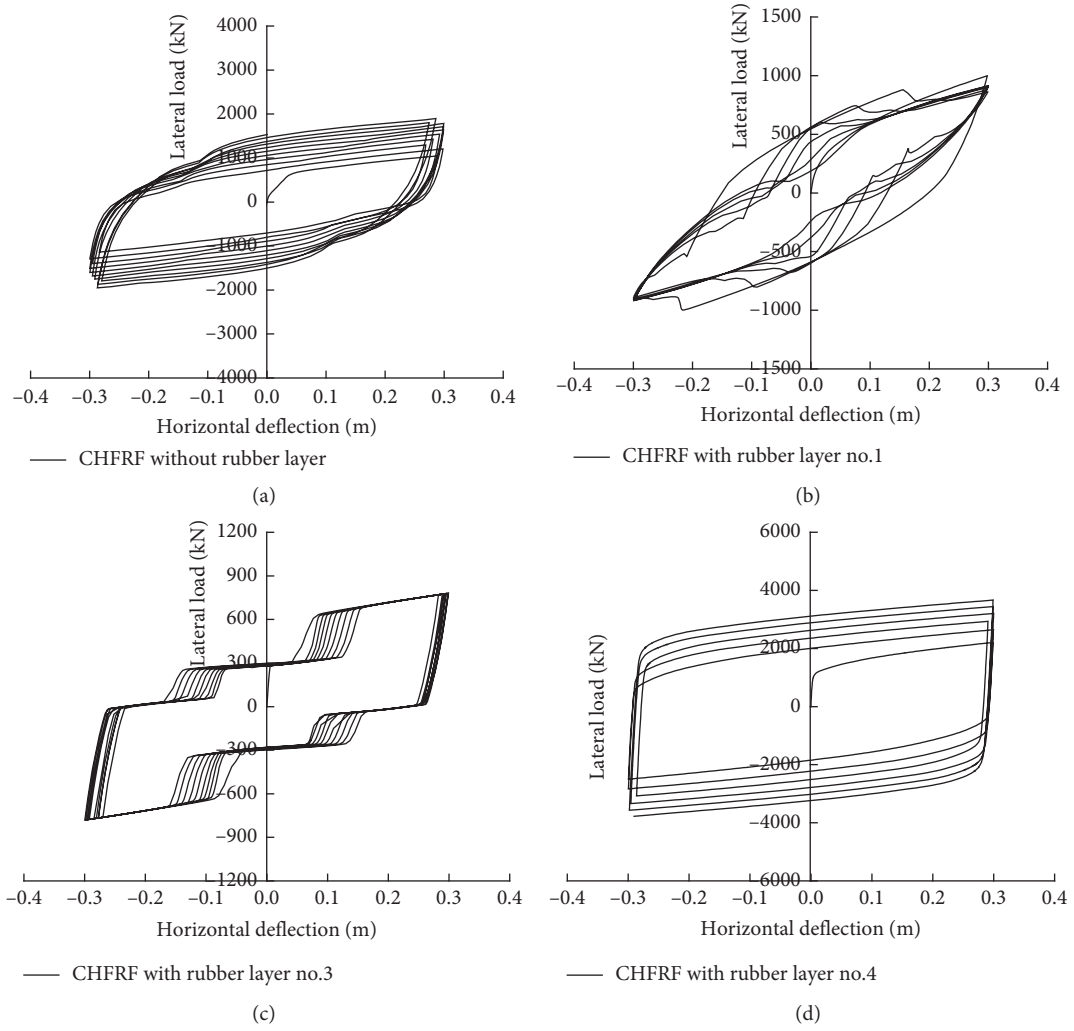

Figure 19: Effects of rubber layer on the lateral bearing capacity. (a) CHFRF without rubber layer. (b) CHFRF with rubber layer no.1. (c) CHFRF with rubber layer no.3. (d) CHFRF with rubber layer no.4.

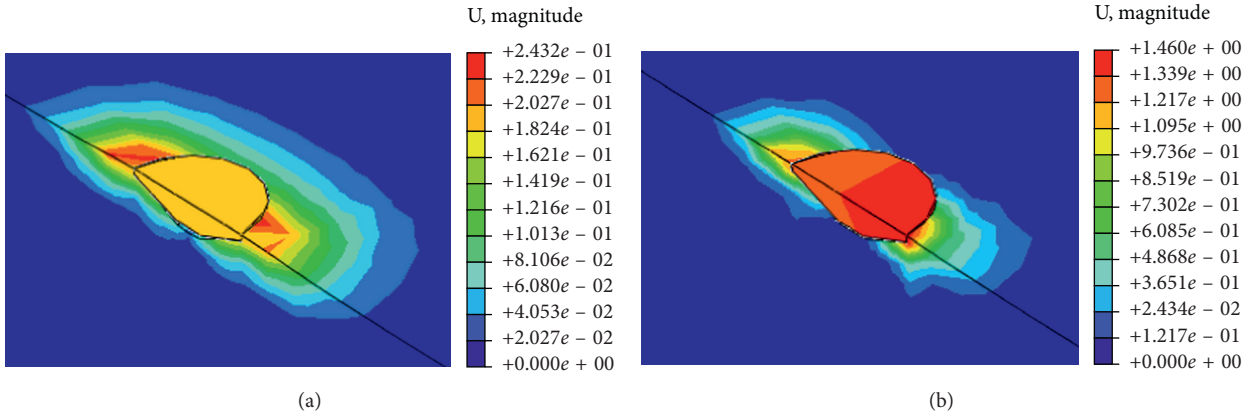

Figure 20: Deformation of the sand surrounding the CHFRF. (a) CHFRF without the rubber layer. (b) CHFRF with the rubber layer no. 4.

buffering the lateral loads and then reduces damage of the foundation and the soil subjected to lateral cyclic loading. Therefore, it is concluded that the CHFRF with the rubber layer that has steel inside outperforms the CHFRF without the rubber layer.

6. Conclusions

An analysis on the effects and affecting factors of bearing behaviors for the CHFRF in sand under lateral loading was conducted by model tests and FEM simulations, covering the lateral bearing capacity, the distributions of the rotation center, and earth pressure, respectively. The effects of rubber layer along the wall of CHFRF on lateral bearing capacity and energy dissipation capacity of the foundation were revealed as well. Thus, the following conclusions can be made:

(1) During lateral loading, the rotation center of the CHFRF gradually moves upwards with the load increasing and also moves to the side of the loading directions. In the ultimate state, the rotation center is located at a depth of about 0.6–0.65 times the foundation height and is 0.15–0.18 times the diameter of the foundation away from its centerline as well.

(2) The results show that the superstructure of the CHFRF is the main part for bearing loads under lateral loading, and the lateral bearing capacity of CHFRF significantly increases with the increase of vertical load and the embedded depth. Besides, the thickness of the rubber and steel included in the rubber layer along the wall of CHFRF is an important factor influencing the lateral bearing capacity.

(3) The rubber layer installed between the wall of CHFRF and the surrounding ground decreases the earth pressure and the deformed range of sand surrounding the foundation, revealing that it can reduce the loads transferred to the soil surrounding the foundation for improving the service life of the foundation. Besides, the rubber layer increases energy dissipation of the foundation compared with the CHFRF without the rubber layer, especially in the case of the rubber layer with steel inside. However, for the CHFRF under lateral cyclic loading in sand, energy dissipation mainly comes from the steel of the rubber layer rather than rubber.

In addition, it should be noted that the objective that rubber included in the rubber layer is used to significantly increase energy dissipation of the CHFRF in sand is not achieved, while it may be achieved in the case of the rock mass. Moreover, the optimal thickness and stiffness of the rubber layer should be further analyzed to obtain enough bearing capacity and foundation stiffness under various loading cases.

Data Availability

The data used to support the findings of this study are included within the article.

Conflicts of Interest

The authors declare that there are no conflicts of interest regarding the publication of this paper.

Acknowledgments

This work was jointly supported by Weifang University Research Fund (Grant no. 2019BS18), the SDUST Research Fund (Grant no. 2015TDJH104), and Opening Foundation of Shandong Key Laboratory of Civil Engineering Disaster Prevention and Mitigation (CDPM2019ZR03).

References

[1] Y. Wan, C. Q. Fan, Y. S. Dai et al., "Assessment of the joint development potential of wave and wind energy in the south China sea," *Energies*, vol. 11, no. 2, p. 398, 2018.

[2] B. K. Sahu, "Wind energy developments and policies in China: a short review," *Renewable and Sustainable Energy Reviews*, vol. 81, pp. 1393–1405, 2018.

[3] Q. C. Zhong, Y. Ping, and B. J. Hai, "Reliability of gravity foundation in coral sands subject to dynamic wind load," *Applied Mechanics and Materials*, vol. 302, pp. 355–358, 2013.

[4] X. Chen, C. F. Li, and J. Z. Xu, "Failure investigation on a coastal wind farm damaged by super typhoon: a forensic engineering study," *Journal of Wind Engineering & Industrial Aerodynamics*, vol. 147, pp. 132–142, 2016.

[5] K. S. Lee and H. J. Bang, "A study on the prediction of lateral buckling load for wind turbine tower structures," *International Journal of Precision Engineering and Manufacturing*, vol. 28, no. 10, 2012.

[6] G. Sivapalan and L. K. Bruce, "Effects of moment-to-shear ratio on combined cyclic load-displacement behavior of shallow foundations from centrifuge experiments," *Journal of Geotechnical and Geoenvironmental Engineering*, vol. 135, no. 8, pp. 1044–1055, 2009.

[7] D. Y. Li, S. S. Li, and Y. K. Zhang, "Cone-shaped hollow flexible reinforced concrete foundation (CHFRF)-Innovative for mountain wind turbines," *Soils and Foundations*, vol. 59, no. 5, pp. 1172–1181, 2019.

[8] S. Gajan and B. L. Kutter, "Contact interface model for shallow foundations subjected to combined cyclic loading," *Journal of Geotechnical and Geoenvironmental Engineering*, vol. 135, no. 3, pp. 407–419, 2009.

[9] S. Adhikari and S. Bhattacharya, "Dynamic analysis of wind turbine towers on flexible foundations," *Shock and Vibration*, vol. 19, no. 1, pp. 37–56, Article ID 408493, 2018.

[10] Q.-F. Gao, H. Dong, Z.-W. Deng, and Y.-Y. Ma, "Wind-induced dynamic amplification effects on the shallow foundation of a horizontal-axis wind turbine," *Computers and Geotechnics*, vol. 88, pp. 9–17, 2017.

[11] L. Govoni, S. Gourvenec, and G. Gottardi, "Centrifuge modelling of circular shallow foundations on sand," *International Journal of Physical Modelling in Geotechnics*, vol. 10, no. 2, pp. 35–46, 2010.

[12] L. Govoni, S. Gourvenec, and G. Gottardi, "A centrifuge study on the effect of embedment on the drained response of shallow foundations under combined loading," *Géotechnique*, vol. 61, no. 12, pp. 1055–1068, 2011.

[13] W. Mohamed and P.-E. Austrell, "A comparative study of three onshore wind turbine foundation solutions," *Computers and Geotechnics*, vol. 94, pp. 46–57, 2018.

[14] A. B. Cerato, "Scale effects of shallow foundation bearing capacity on granular materia," *Journal of Geotechnical and Geoenvironmental Engineering*, vol. 133, no. 10, pp. 1192–1202, 2007.

[15] L. Décourt, "Design of shallow foundations on soils and rocks on basis of settlement considerations," *Geotechnical Special Publication*, vol. 299, pp. 342–357, 2018.

[16] M. J. Vahdatirad, D. V. Griffiths, L. V. Andersen, and G. A. Fenton, "Reliability analysis of a gravity-based foundation for wind turbines: a code-based design assessment," *Geotechnique*, vol. 64, no. 8, pp. 635–645, 2014.

[17] D. Li, L. Feng, and Y. Zhang, "Model tests of modified suction caissons in marine sand under monotonic lateral combined loading," *Applied Ocean Research*, vol. 48, pp. 137–147, 2014.

[18] ASTM, "Standard test method for density, relative density (specic gravity), and absorption of coarse aggregate," pp. 237–280, ASTM International, Philadelphia, PA, USA, 2017, Tech. Rep. ASTM C127–07.

[19] A. W. Skempton, "Standard penetration test procedures and the effects in sands of overburden pressure, relative density, particle size, ageing and overconsolidation," *Geotechnique*, vol. 36, no. 3, pp. 411-412, 1986.

[20] R. B. Kelly, G. T. Houlsby, and B. W. Byrne, "A comparison of field and laboratory tests of caisson foundations in sand and clay," *Géotechnique*, vol. 56, no. 9, pp. 617–626, 2006.

[21] D. Y. Li, S. S. Li, and Y. K. Zhang, "Earth pressure distribution and sand deformation around modified suction caissons (MSCs) under monotonic lateral loading," *China Ocean Engineering*, vol. 33, no. 22, pp. 1–9, 2019.

[22] D. Li, Y. Zhang, L. Feng, and Y. Gao, "Capacity of modified suction caissons in marine sand under static horizontal loading," *Ocean Engineering*, vol. 102, pp. 1–16, 2015.

[23] A. C. Bassi, F. Casa, and R. Mendichi, "Shore A hardness and thickness," *Polymer Testing*, vol. 7, no. 3, pp. 165–175, 1987.

[24] C. B. Mary and M. A. Ellen, "Constitutive models of rubber elasticity: a review," *Rubber Chemistry and Technology*, vol. 73, no. 3, pp. 504–523, 2000.

[25] L. L. Wang and T. Ishihara, "A study of the effects of foundation uplift on the seismic loading of wind turbine tower and shallow foundation using a new dynamic Winkler model," *Engineering Structures*, vol. 219, Article ID 110745, 2020.

[26] S. S. Li and D. Y. Li, "Mechanical properties of scrap tire crumbs-clayey soil mixtures determined by laboratory tests," *Advances in Materials Science and Engineering*, vol. 2018, Article ID 1742676, 10 pages, 2018.

[27] M. M. Heydari, M. R. Ayatollahi, M. Dehghany, and F. Berto, "Mixed-mode (I/II) failure assessment of rubber materials using the effective stretch criterion," *Theoretical and Applied Fracture Mechanics*, vol. 91, pp. 126–133, 2017.

[28] S. Mukherjee, "A theoretical study and 3D modeling of nonlinear passive vibration isolator," *International Journal of Applied and Advanced Scientific Research*, vol. 2, no. 2, pp. 1–10, 2017.